# UC San Diego
## UC San Diego Previously Published Works

**Title**

Neuron-targeted caveolin-1 improves neuromuscular function and extends survival in SOD1G93A mice

**Permalink**

**Journal**

**ISSN**

**Authors**

Sawada, Atsushi
Wang, Shanshan
Jian, Minyu
et al.

**Publication Date**

**DOI**

# Neuron-targeted caveolin-1 improves neuromuscular function and extends survival in SOD1$^{G93A}$ mice

Atsushi Sawada,*,†,‡ Shanshan Wang,*,† Minyu Jian,*,†,§ Joseph Leem,*,† Jesse Wackerbarth,*,† Junji Egawa,*,†,¶ Jan M. Schilling,*,† Oleksandr Platoshyn,†,‖ Alice Zemljic-Harpf,*,† David M. Roth,*,† Hemal H. Patel,*,† Piyush M. Patel,*,† Martin Marsala,†,‖ and Brian P. Head*,†,1

*Veterans Affairs San Diego Healthcare System, San Diego, California, USA; †Department of Anesthesiology, School of Medicine, University of California–San Diego, La Jolla, California, USA; ‡Department of Anesthesiology, Sapporo Medical University, Sapporo, Japan; §Department of Anesthesiology, Beijing Tiantan Hospital, Capital Medical University, Beijing, China; ¶Department of Anesthesiology, Nara Medical University, Kashihara, Japan; and ‖Sanford Consortium for Regenerative Medicine, La Jolla, California, USA

**ABSTRACT:** Interventions that preserve motor neurons or restore functional motor neuroplasticity may extend longevity in amyotrophic lateral sclerosis (ALS). Delivery of neurotrophins may potentially revive degenerating motor neurons, yet this approach is dependent on the proper subcellular localization of neurotrophin receptor (NTR) to plasmalemmal signaling microdomains, termed membrane/lipid rafts (MLRs). We previously showed that overexpression of synapsin-driven caveolin-1 (Cav-1) (*SynCav1*) increases MLR localization of NTR [*e.g.*, receptor tyrosine kinase B (TrkB)], promotes hippocampal synaptic and neuroplasticity, and significantly improves learning and memory in aged mice. The present study crossed a SynCav1 transgene–positive (SynCav1$^+$) mouse with the mutant human superoxide dismutase glycine to alanine point mutation at amino acid 93 (hSOD1$^{G93A}$) mouse model of ALS. When compared with hSOD1$^{G93A}$, hSOD1$^{G93A}$/SynCav1$^+$ mice exhibited greater body weight and longer survival as well as better motor function. Microscopic analyses of hSOD1$^{G93A}$/SynCav1$^+$ spinal cords revealed preserved spinal cord α-motor neurons and preserved mitochondrial morphology. Moreover, hSOD1$^{G93A}$/SynCav1$^+$ spinal cords contained more MLRs (cholera toxin subunit B positive) and MLR-associated TrkB and Cav-1 protein expression. These findings demonstrate that *SynCav1* delays disease progression in a mouse model of ALS, potentially by preserving or restoring NTR expression and localization to MLRs.—Sawada, A., Wang, S., Jian, M., Leem, J., Wackerbarth, J., Egawa, J., Schilling, J. M., Platoshyn, O., Zemljic-Harpf, A., Roth, D. M., Patel, H. H., Patel, P. M., Marsala, M., Head, B. P. Neuron-targeted caveolin-1 improves neuromuscular function and extends survival in SOD1$^{G93A}$ mice. FASEB J. 33, 7545–7554 (2019). www.fasebj.org

**KEY WORDS:** neuroplasticity · motor neurons · MLR · TrkB · mitochondria

Amyotrophic lateral sclerosis (ALS) derives its name from denervational atrophy of the muscles in the tongue, oropharynx, and limbs (amyotrophy), degenerating corticospinal axons resulting in thinning and scarring (sclerosis) of the lateral spinal cord, and thinning of the ventral roots. ALS, known colloquially in the United States as Lou Gehrig's disease, is a progressive neurodegenerative disease resulting from loss of upper and lower motor neurons in the brain, brain stem, and spinal cord, accompanied by a 2–5-yr life expectancy (1–4). Incidence of ALS is 3–5 per 100,000 persons globally and is present in both dominantly inherited familial ALS (FALS, 5–10%) and sporadic ALS (SALS, 90–95%) forms (1, 4). Typical age of onset is 58–63 and 47–52 yr for SALS and FALS, respectively, with both being phenotypically similar.

To date, the only U.S. Food and Drug Administration–approved treatments for ALS are Rilutek (riluzole) (3) and Radicava (edaravone) (5), with both demonstrating modest improvements. For FALS, genetic interventions are focused on knocking down key genes such as a mutant form of super oxide dismutase 1 (*SOD1*) (6). However, because of the lesser-known etiology of SALS, interventions that are neuroprotective or promote neuroplasticity

need to be adopted. Interventions (gene therapy combined with pharmacology) that restore neuromuscular function may extend life span and improve the quality of life for individuals afflicted with ALS.

ALS is a multicomplex disease attributed to decreased neurotrophic support and loss of neurotrophin receptor (NTR) signaling (7, 8), diffuse muscle weakness, muscle atrophy, spasticity, hyperreflexia (upper), and paralysis (lower) (3, 4). Exogenous delivery of neurotrophins is emerging as an attractive therapeutic approach for ALS (2), yet effective neurotrophin signaling is dependent on the proper subcellular localization of NTRs to plasma membrane signaling microdomains, termed membrane/lipid rafts (MLRs) (9–12). Genetic interventions that enhance MLR localization of NTRs *in vivo* (13) may serve to preserve motor neuron function and/or increase the efficacy of endogenous neurotrophins or exogenous delivery of NTR agonists to improve function in ALS.

We have previously shown that caveolin-1 (Cav-1), a MLR-scaffolding protein (12), is neuroprotective (14), increases receptor tyrosine kinase B (TrkB) signaling *in vitro* (15) and MLR localization of TrkB *in vivo* (13), and augments neurotrophin signaling. Moreover, intraparenchymal delivery of neuron-targeted Cav-1 [using a neuron-specific synapsin promoter, synapsin-driven Cav-1 (*SynCav1*)] enhances structural and functional hippocampal neuroplasticity and significantly improves hippocampal-dependent learning and memory in both adult and aged mice (13). Whether *SynCav1* can prevent neurodegeneration and preserve neuromuscular function in a disease model like ALS has not been studied. To test this, we crossed our SynCav1 transgenic mouse with the human superoxide dismutase glycine to alanine point mutation at amino acid 93 (hSOD1$^{G93A}$) mouse and assessed longevity, neuromuscular function, motor neuronal survival, and mitochondrial morphology. hSOD1$^{G93A}$/SynCav1 mice demonstrated preserved body weight and longer survival, greater motor-evoked potentials (MEPs), better running wheel performance, preserved motor neuron survival, and normal mitochondrial morphology. Furthermore, hSOD1$^{G93A}$/SynCav1 spinal cords expressed more MLRs [cholera toxin subunit B (CT-B) positive] and MLR-localized TrkB and Cav-1 protein expression.

## MATERIALS AND METHODS

All animals were treated in compliance with the *Guide for the Care and Use of Laboratory Animals* [National Institutes of Health (NIH), Bethesda, MD, USA]. All animal use protocols were approved by the Veterans Administration San Diego Healthcare System Institutional Animal Care and Use Committee (San Diego, CA, USA) prior to performed procedures. Transgenic mice expressing ALS-linked human SOD1 mutant protein (hSOD1$^{G93A}$) exhibit an ALS-like neurodegenerative phenotype characterized by diminished body weight from muscle atrophy, weakness and/or paralysis, fasciculations, and early death, along with reductions in functional cortical-α motor neurons and ventral horn-α motor neurons that can be observed histologically (16, 17). The transgenic model used for this current study, determination of disease onset, progression, and end stage as well as histologic assessment

of the lumbar spinal cord were based on the *Guidelines for Preclinical Animal Research in ALS/MND* (18).

## hSOD1$^{G93A}$ mouse genotyping

The hSOD1$^{G93A}$ transgenic male mice were obtained from Dr. Cleveland's laboratory [University of California– San Diego (UCSD), La Jolla, California] and bred on SynCav1 transgenic female mice to produce wild-type [or transgene-negative (Tg-neg)], SynCav1 transgene–positive (SynCav1$^+$), hSOD1$^{G93A}$-positive, and hSOD1$^{G93A}$/SynCav1$^+$ double-positive mice. Transgenic mice were genotyped by PCR amplification on tail biopsy samples taken at the time of weaning (at 3 wk of age). hSOD1$^{G93A}$-positive mice were confirmed using the following primers: primer 1, mouse (m)SOD1 [5'-GTT-ACATATAGGGGTTTACTTCATAATCTG-3' (132647786)]; primer 2, hSOD1 [5'-CCAAGATGCTTAACTCTTGTAATCAA-TGGC-3' (132647787)]; and primer 3, human (h)/mSOD1 [5'-CAGCAGTCACATTGCCCAAGGTCTCCAACATG-3' (132647788)]. These primers were used to detect a product size of 800 and 600 base pair (bp) for mouse and human SOD1, respectively. SynCav1 transgenic mice were generated in C57BL/6 background through the UCSD mouse transgenic core (19). Full-length Cav-1 cDNA (537 bp) was cloned into a vector containing the human neuron-specific synapsin promoter (495 bp) (20) and termed *SynCav1* as previously described in refs. 15 and 19. SynCav1$^+$ mice were confirmed using the following primer sequences, which overlapped a portion of synapsin and Cav1 cDNA to generate a product size of 470 bp: SynCav1 forward [5'-CAGCTTCAGCACCGCGGACA-3' (138389038)] and SynCav1 reverse [5'-CACCTCGTCTGC-CATGGCCT-3' (138389039)] (Supplemental Fig. S1). PCR products were separated on a 1% agarose gel and run for 35 min at 135 V. All mouse strains were generated on the C57BL/6 background.

## Behavior

### Kaplan-Meier survival

Survival analyses were performed using Kaplan-Meier analyses. Survival endpoint is defined by the inability of the mouse to right itself within 30 s on its back, a humane endpoint that guarantees that animals are euthanized before they are unable to forage for food for water (17, 21).

### Voluntary wheel running

Mice were housed individually in plastic cages measuring 35.3 × 23.5 × 20 cm (length × width × height) with a 12.7 cm diameter running wheel mounted in the cage top (model 80821S; Lafayette Instrument, Lafayette, IN, USA). The mice had open access to running wheels within each cage under conditions of a 12-h light/dark cycle (lights of from 5 AM to 5 PM). The duration of experiment was 36 h, including 2 dark cycles. A mechanical counter was used to record wheel rotations and was connected to a desktop computer *via* Activity Wheel Monitoring Software (model 86065; Lafayette Instrument). The software analyzed running velocity (m/min), distance (m/h), and total distance (m). The mice had access to food and water *ad libitum* and were checked daily for health and wellness.

## Electrophysiology

### Electromyography

Under isoflurane anesthesia with 2% in room air, we recorded resting electromyography (EMG) by 30-gauge platinum transcutaneous needle-recording electrodes positioned in the

gastrocnemius muscle in all animals (distance between recording electrode, ~7 mm). A ground electrode was subcutaneously placed in the back. Electrodes were connected to an active headstage (Warner Instruments, Hamden, CT, USA), signal-amplified recorded using DP-311 differential amplifier (Warner Instruments), digitalized by the PowerLab 8/30 Data Acquisition System (ADInstruments, Sydney, Australia) at a sampling frequency of 20 kHz, and digitized and stored using LabChart 7 (ADInstruments) in PC for analysis.

### MEPs

To measure MEPs, mice were anesthetized by intraperitoneal injection of propofol (20 mg/kg for mice). Two 30-gauge stimulating electrodes were placed subcutaneously overlying the left and right motor cortex. In all mice, MEPs of lower limb recorded by 30-gauge platinum transcutaneous needle from the gastrocnemius muscle (distance between recording electrode, ~7 mm) were elicited in all mice by transcranial electrical stimulation with a pulse duration of 800 μs at 15 mA using a DS3 constant current isolated stimulator (Digitimer, Welwyn Garden City, United Kingdom), and MEPs of upper limb recorded by 30-gauge platinum transcutaneous needle from the trapezius muscle (distance between recording electrode, ~5 mm) were elicited with a pulse duration of 800 μs at 3 mA. Recording electrodes were connected to an active headstage (Warner Instruments) and signal-amplified recorded (×100) using DP-311 differential amplifier (Warner Instruments). Amplified signal was acquired by the PowerLab 8/30 Data Acquisition System (ADInstruments) at a sampling frequency of 20 kHz, and digitized and stored using LabChart 7 (ADInstruments) in PC for analysis.

## Microscopy

### Immunofluorescence confocal microscopy

After electrophysiological recording, animals were anesthetized with intraperitoneal injections of sodium pentobarbital (50 mg/kg) and transcardially perfused with PBS, followed by 4% paraformaldehyde. Spinal cord was postfixed in paraformaldehyde overnight and stored in 30% sucrose. The third cervical vertebral spinal column (C3), first thoracic vertebral spinal column (T1), and fourth lumbar vertebral spinal column (L4) segments of spinal cords were cut into serial 20-μm coronal sections in a cryostat and collected as free-floating sections for immunohistochemistry. Tissue sections were incubated with primary antibodies for choline acetyltransferase (ChAT; 1:200, AB144P; MilliporeSigma, Burlington, MA, USA) and Cav-1 (3267, 1:500; Cell Signaling Technology, Danvers, MA, USA) overnight at 4°C. Sections were then incubated for 1 h with Alexa Fluor 488-conjugated or Alexa Fluor 594–conjugated secondary antibody at a dilution of 1:500 (Thermo Fisher Scientific, Waltham, MA, USA). Nuclei were counterstained with DAPI dihydrochloride solution (D523, 1:1000; Dojindo, Kumamoto, Japan). Images were captured using confocal laser microscopy (A1; Nikon, Tokyo, Japan). Every third section from each spinal cord segment was stained with ChAT immunohistochemistry and DAPI nuclear staining. ChAT-positive round-shaped cells with maximum diameters >40 μm were counted at both sides of the spinal dorsal horns to determine the number of α motor neurons by confocal laser microscopy at ×40 magnification (A1; Nikon). Maximum diameter of cells and immunofluorescence of ChAT and DAPI were measured using ImageJ software (NIH). The mean numbers of ChAT-positive round-shaped cells in every third section were used for analysis.

### Electron microscopy

Mice were transcardially perfused with 2% glutaraldehyde, treated with 1% OsO$_4$, and were *en bloc* stained with uranyl acetate. For flat embedding of the vertebral column 4 lumbar sections, thin flexible molds were employed to lay the sections as level as possible in LX112 embedding medium (MilliporeSigma) and then overlayed with plastic coverslips. Semithin sections (0.5) of the right hemisphere of the vertebral column embedded in resin were stained with toluidine blue, an alkaline solution that stains acidic tissue components such as nucleic acids. Toluidine blue allows for identification of structural details used for electron microscopy (EM). Flat embedded blocks were visually trimmed (based on toluidine blue stain) to the ventral horn regions located in the L4 vertebral column and thin sectioned to 70 nm. Grids were viewed unstained using an FEI Tecnai EM Scope (FEI, Hillsboro, OR, USA). Motor neuronal cell bodies were used as a visual tissue reference to then locate proximal myelinated fibers that correspond to comparable motor regions within the ventral horn. Only mitochondria located within myelinated fibers were used for analyses. Approximately 5 micrographs at ×4800 magnification (each representing 5 separate regions of ~1 μm$^2$ in area) per animal (3 animals) were used to perform the analyses. Approximately 140–160 total mitochondria per group (compiled from 3 separate mice) were used in the analyses for area and perimeter, and ~40 were used to measure cristae area and mitochondria (higher magnification contained less mitochondria per micrograph). Alterations in mitochondrial morphology were measured using Adobe Photoshop (San Jose, CA, USA) to determine cristae density fraction, mitochondrial perimeter, and area as previously described in refs. 22 and 23.

### Biochemical isolation of MLRs

After completion of behavioral tests, mice were euthanized by decapitation, and spinal cord tissue was dissected on ice and homogenized at 4°C with carbonate lysis buffer (500 mM sodium carbonate, pH 11.0) containing protease inhibitor and phosphatase inhibitor. After homogenization, the samples were sonicated on ice for 3 times for 15 s each. The nuclear components were removed by centrifugation at 1000 *g* for 10 min, and the protein concentration was quantified by Bradford assay and normalized to 0.4 mg/ml for later use. Sucrose was dissolved in 2-(*N*-morpholino)ethanesulfonic acid (MES) buffered saline (25 mM MES and 150 mM NaCl, pH 6.5) buffer to prepare 80, 35, and 5% solutions. Sucrose gradients were prepared by adding 1 ml of 80% sucrose followed by 1 ml of sonicated sample with brief vortexing and then layering 6 ml of 35% sucrose and 4 ml of 5% sucrose. Gradients were ultracentrifuged using a SW-41 rotor (Beckman Coulter, Brea, CA, USA) at 39k rpm for 17 h at 4°C. Fractions (1 ml) were collected from the top of each tube starting at 4–12 ml. Samples were run as individual fractions 4–12 and subjected to immunoblot analysis. Buoyant fractions 4 and 5 (*i.e.*, MLR fractions) are found at the 5/35% interface based on their lipid components and biophysical properties as previously described in refs. 13 and 24. Electrophoresis was performed on the samples using 4–12% acrylamide gels (Thermo Fisher Scientific) and transferred to PVDF membranes (MilliporeSigma) by electroelution. Membranes were blocked in blocking solution [20 mM Tris-buffered saline with Tween 20 (TBST) (0.1%) containing 3% bovine serum albumin] and then incubated with primary antibodies Cav-1 (3238; 1:1000; Cell Signaling Technology), TrkB (610102; 1:1000; BD Biosciences, San Jose, CA, USA), and CT-B (C-22841, 1:1000; Thermo Fisher Scientific) overnight at 4°C as previously described in Egawa *et al.* (19). After 3 washes with TBST, the membrane was incubated with species-specific infrared-dye–labeled secondary antibody for 1 h at room temperature in dark. After another 3 times wash with TBST to remove the rest of the secondary antibody, membrane was washed by Tris-buffered saline one more time to remove the Tween residual to avoid background. Densitometric analysis (arbitrary units) of fraction

samples were normalized to protein concentration in spinal cord homogenates, and MLR fractions 4 and 5 were compared with wild type.

## Statistics

Statistical analysis was performed with Prism 7 software (GraphPad, La Jolla, CA, USA). When appropriate, statistical analysis of means ± SEM differences between groups was performed by a Student's $t$ test or 2-way ANOVA repeated measures, followed by Bonferroni or Tukey's multiple comparison *post hoc* analysis. The Kaplan-Meier survival curve was analyzed using a log-rank test. Mean and median survival were analyzed by an unpaired Student's $t$ test. Significance was assumed when $P < 0.05$. All experimental groups were blinded, and code was broken only for analysis.

## RESULTS

### SOD1[G93A]/SynCav1^{+} mice exhibit preserved body weight and greater longevity

We have previously shown that neuron-targeted Cav-1 (*i.e.*, SynCav1) enhances prosurvival and progrowth signaling *in vitro* (15) and improves functional neuroplasticity *in vivo* (13); therefore, we tested whether a SynCav1 transgenic mouse could delay disease progression in an hSOD[G93A] ALS mouse model. Body weight measurements revealed a significant interaction [2-way ANOVA, $F$ (12, 684) = 11.41, $P < 0.0001$], time effect [$F$ (8, 684) = 12.21, $P < 0.0001$], and gene effect [$F$ (3, 684) = 89.22, $P < 0.0001$] (**Fig. 1A**). Similar to previously published works demonstrating weight loss at 11 wk [77 d, as reported in Zhong *et al.* (17)], when compared with Tg-neg, SOD1[G93A] mice exhibited significant weight loss starting at 12 wk (Tukey's *post hoc*, $P < 0.0001$) with a maximum 23% drop at 17 wk (relative to maximum weight at 10 wk). In contrast, hSOD1[G93A]/SynCav1^{+} mice never exhibited >6% weight loss at any time point (5.3%
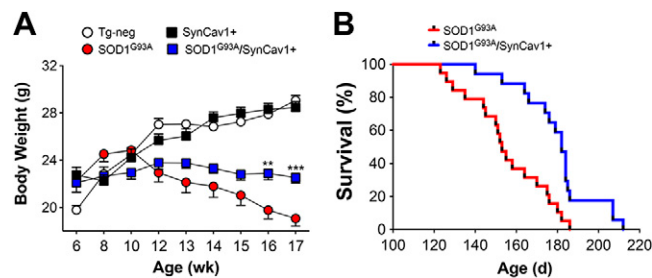
**Figure 1.** SOD1[G93A]/SynCav1^{+} mice exhibit preserved body weight and greater longevity. *A*) Body weight curves for Tg-neg, SynCav1^{+}, SOD1[G93A], and SOD1[G93A]/SynCav1^{+} ($n = 20$/group). Data are expressed as means ± SEM. **$P < 0.01$, ***$P < 0.001$ *vs.* SOD1[G93A]. Two-way ANOVA with Tukey's multiple comparisons *post hoc* test with significance set at $P < 0.05$. *B*) Kaplan-Meier survival curve of male SOD1[G93A] ($n = 19$) and SOD1[G93A]/SynCav1^{+} ($n = 17$) mice. Mean survival (mean ± SEM): SOD1[G93A]/SynCav1^{+}, 180.3 ± 4.5 d; SOD1[G93A], 155.5 ± 4.4 d; $P = 0.0004$, unpaired Student's $t$ test. Median survival: SOD1[G93A]/SynCav1^{+}, 182 d; SOD1[G93A], 153 d; $P = 0.0006$, unpaired Student's $t$ test (log-rank Mantel-Cox test).
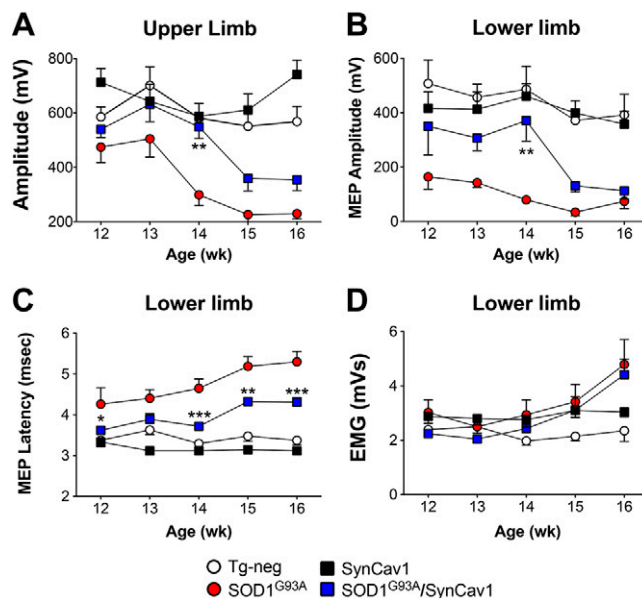
**Figure 2.** SOD1[G93A]/SynCav1^{+} mice exhibit greater MEPs in upper and lower limbs. To identify conductivity of descending motor axons, MEPs were elicited by electrical stimulation of motor cortex and extrapyramidal system and responses recorded in upper trapezius or lower gastrocnemius muscles. *A*) Amplitude of MEP from upper limb. *B*) Amplitude (mV) of MEP from lower limb (gastrocnemius muscle). *C*) Latency (ms) of MEP from lower limb. *D*) Resting EMG (mVs) from lower limb. Two-way ANOVA with Tukey's multiple comparison *post hoc* test. All data are expressed as means ± SEM. ($n = 9$–10/group). *$P < 0.05$, **$P < 0.01$, ***$P < 0.001$ *vs.* SOD1[G93A].

weight loss at 17 wk when compared with maximum weight at 12 wk). Tukey's *post hoc* revealed that hSOD1[G93A]/SynCav1^{+} mice had significantly greater body weight than hSOD1[G93A] at 16 ($P = 0.003$) and 17 wk ($P = 0.0006$) (Fig. 1A). Kaplan-Meier survival curve analysis (Fig. 1B) revealed that hSOD1[G93A]/SynCav1^{+} mice lived significantly longer when compared with hSOD1[G93A] (180.3 ± 4.5 d for hSOD1[G93A]/SynCav1^{+} *vs.* 155.5 ± 4.4 d for hSOD1[G93A]; $P = 0.0004$, mean ± SEM, unpaired Student's $t$ test), with a median survival age of 182 *vs.* 153 d for hSOD1[G93A]/SynCav1^{+} and hSOD1[G93A], respectively ($P = 0.0006$, log-rank Mantel Cox test). At 153 d, 88% (88.2 ± 7.8; longest survival, 212 d) of hSOD1[G93A]/SynCav1^{+} mice survived compared with only 47% (47.4 ± 11.3; longest survival, 186 d) of hSOD1[G93A]. These results demonstrate that hSOD1[G93A]/SynCav1^{+} mice have preserved body weight and live ~1 mo (~19%) longer than hSOD1[G93A] mice.

### hSOD1[G93A]/SynCav1^{+} mice exhibit preserved neuromuscular function

In order to assess the upper motor neuron connectivity at the spinal cord level, MEPs were recorded in the lower gastrocnemius and upper trapezius muscles in all groups at different end stages (**Fig. 2**). MEPs revealed a significant (2-way ANOVA) interaction [$F$ (12,164) = 2.40, $P = 0.007$],

time effect [$F_{(4,164)} = 8.76$, $P < 0.0001$], and gene effect [$F_{(3,164)} = 34.91$, $P < 0.0001$] in upper-limb amplitude (Fig. 2A); a nonsignificant interaction [$F_{(12,164)} = 0.76$, $P = 0.69$], a significant time effect [$F_{(4,164)} = 4.67$, $P = 0.001$], and significant gene effect [$F_{(3,164)} = 36.38$, $P < 0.0001$] in lower-limb amplitude (Fig. 2B); and a significant interaction [$F_{(12,164)} = 2.80$, $P = 0.002$], time effect [$F_{(4,164)} = 5.49$, $P = 0.0004$], and gene effect [$F_{(3,164)} = 96.39$, $P < 0.0001$] in lower-limb latency (Fig. 2C). Tukey's *post hoc* test revealed hSOD1$^{G93A}$/SynCav1$^+$ mice ($n = 10$) exhibited greater upper- ($P = 0.003$) and lower-limb amplitude ($P = 0.002$) at 14 wk as well as shorter lower-limb latency at 14 wk ($P = 0.0002$), 15 wk ($P = 0.001$), and 16 wk ($P = 0.0001$) compared with hSOD1$^{G93A}$ ($n = 9$). EMG (mVs) was significantly greater in hSOD1$^{G93A}$ *vs.* Tg-neg mice (Tukey's *post hoc*, $P = 0.0001$) with no significant difference *vs.* hSOD1$^{G93A}$/SynCav1$^+$ mice at 16 wk (Fig. 2D). These results demonstrate that hSOD1$^{G93A}$/SynCav1$^+$ mice exhibit delayed neuromuscular disease progression by ~1 mo when compared with hSOD1$^{G93A}$ mice.

## hSOD1$^{G93A}$/SynCav1$^+$ mice exhibit better running wheel endurance and preserved α-motor neurons at 12 wk

We next performed a voluntary running wheel test to assess changes in motor function. One-way ANOVA with Tukey's *post hoc* revealed hSOD1$^{G93A}$ mice ($n = 9$) exhibited lower mean velocity [$0.96 \pm 0.15$ m/s; $F_{(3,33)} = 28.7$] and less total distance run [$2123 \pm 340$ m; $F_{(3,33)} = 28.4$] compared with Tg-neg ($4.12 \pm 0.31$ m/s, $P < 0.0001$; $9126 \pm 690$ m, $P = 0.0005$; $n = 9$) and hSOD1$^{G93A}$/SynCav1$^+$ ($2.40 \pm 0.40$ m/s, $P = 0.005$; $5318 \pm 887$ m, $P = 0.005$; $n = 10$) at 12 wk (**Fig. 3A, B**). At 16 wk, hSOD1$^{G93A}$ mice ran significantly slower [$1.4 \pm 0.20$ m/s; 1-

way ANOVA; $F_{(3,33)} = 16.6$ with Tukey's *post hoc*; $P = 0.001$; $n = 9$] and covered less total distance [$3256 \pm 457$ m; 1-way ANOVA; $F_{(3,33)} = 15.1$ with Tukey's *post hoc*; $P = 0.002$] compared with Tg-neg ($3.69 \pm 0.37$ m/s; $8254 \pm 823$; $n = 9$) (Fig. 3C); there was no significant difference in mean velocity or total distance run between hSOD1$^{G93A}$ and hSOD1$^{G93A}$/SynCav1$^+$ mice ($1.49 \pm 0.28$ m/s, $P = 0.99$; $3622 \pm 671$, $P = 0.99$; $n = 10$) at 16 wk (Fig. 3E, F). No significant difference was observed among the 4 groups at 8 wk (Supplemental Fig. S2A).

Immunofluorescence confocal microscopy (**Fig. 4A**) revealed less ChAT-positive α-motor neurons in the thoracic [1-way ANOVA with Tukey's *post hoc*, $F_{(3,12)} = 0.497$; $P = 0.008$] and lumbar [$F_{(3,12)} = 0.497$; $P = 0.003$] but not cervical (Fig. 4B) [$F_{(3,12)} = 0.502$; $P = 0.2$; $n = 4$/group] ventral horns of SOD1$^{G93A}$ mice at 12 wk; hSOD1$^{G93A}$/SynCav1$^+$ mice ($n = 4$) had significantly more α-motor neurons in thoracic ($P = 0.02$; Fig. 4B) and lumbar ($P = 0.006$; Fig. 4C) ventral horns at 12 (Fig. 4D) but not at 16 wk (Supplemental Fig. S3). Compared with Tg-neg, there was a measurable loss of cervical ventral horn motor neurons from SOD1$^{G93A}$ mice at 16 wk [1-way ANOVA, $F_{(3,12)} = 1.56$; $P = 0.001$; with Tukey's *post hoc*; $P = 0.002$], an indicator of disease progression within the spinal cord. Immunofluorescence confocal microscopy and running wheel data show that hSOD1$^{G93A}$/SynCav1$^+$ mice exhibit an ~1-mo delay in disease progression regarding motor neuron death and motor function, respectively.

## hSOD1$^{G93A}$/SynCav1$^+$ mice have increased MLR and MLR-localized TrkB in spinal cord tissue

There is evidence of decreased neurotrophic support and loss of NTR signaling in ALS (7, 8), Although targeting
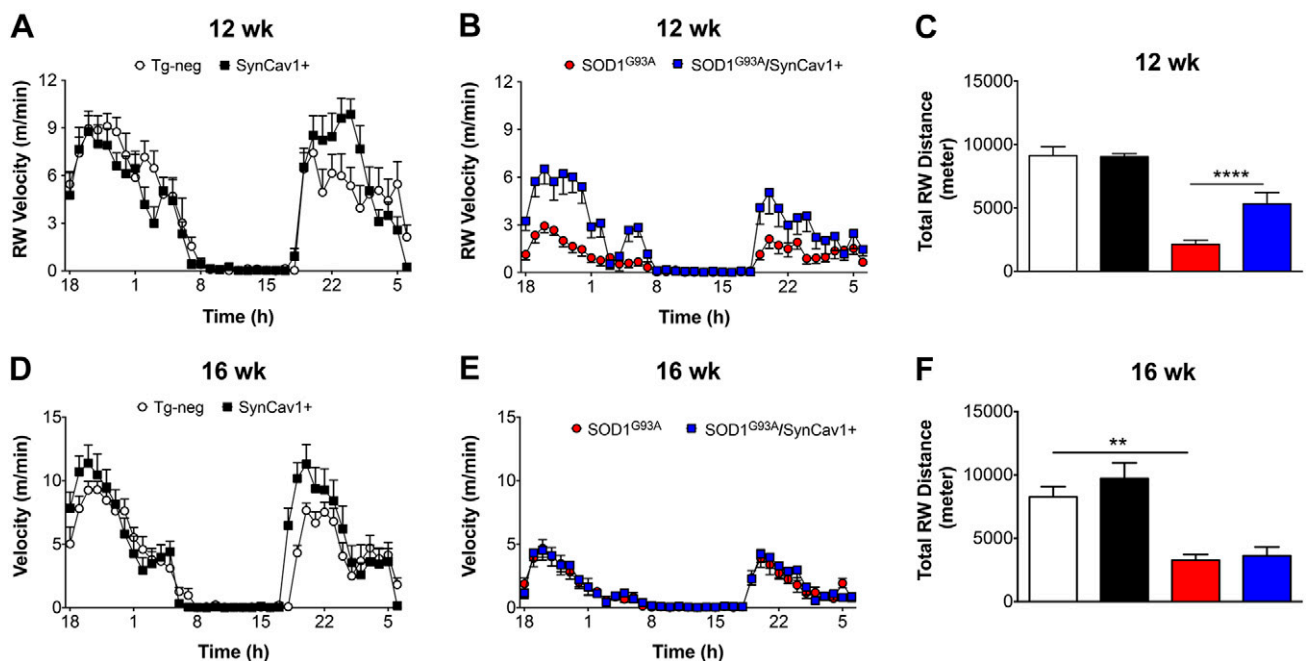


**Figure 3.** SOD1$^{G93A}$/SynCav1$^+$ mice perform better on voluntary running wheel (RW) task. The 12-wk (*A–C*) and 16-wk (*D–F*) mean RW velocity (m/s) and total distance (m) for 36 h. Data are expressed as means ± SEM. ($n = 9$–10/group). One-way ANOVA with Tukey's multiple comparisons *post hoc* test with significance set at $P < 0.05$. **$P < 0.01$, ****$P < 0.0001$.
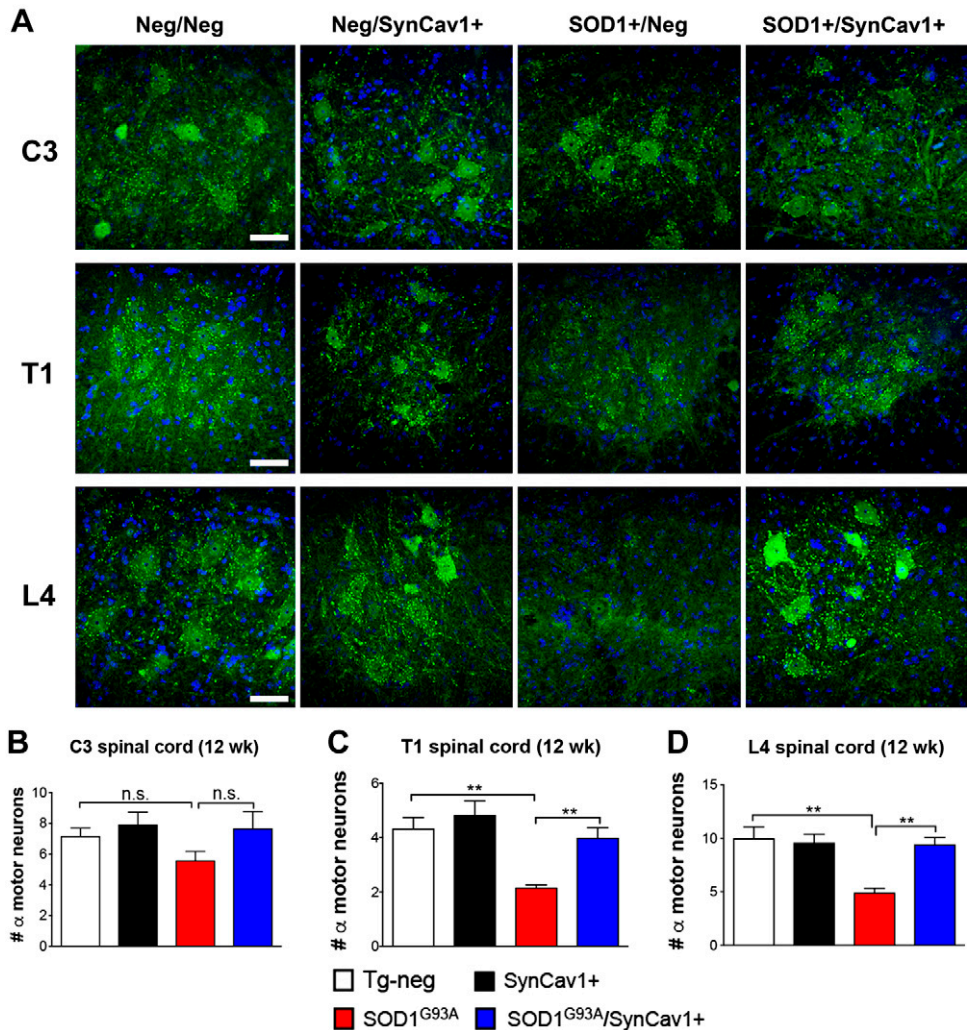
**Figure 4.** SOD1$^{G93A}$/SynCav1$^+$ mice display more ChAT-positive α-motor neurons in spinal ventral horn column at 12 wk. *A*) Immunofluorescence confocal microscopy for ChAT-positive neurons in cervical (C3), thoracic (T1), and lumbar (L4) spinal cord at 12 wk. Scale bars, 50 μm. *B–D*) Quantitation of total number of α-motor neurons in C3 (*B*), T1 (*C*), and L4 (*D*) ventral horn segments from the spinal cord. Data are expressed as means ± SEM. (*n* = 4/group). N.s., not significant. One-way ANOVA with Tukey's multiple comparisons *post hoc* test with significance set at *P* < 0.05. **P* < 0.01.

NTRs offers a potential therapy for ALS (2, 3, 7), NTR signaling is dependent on localization to MLRs (9, 10, 25–28). Because we have previously shown that *SynCav1* delivery to the CNS *in vivo* increases MLR-localized TrkB expression (13), we therefore performed sucrose density fraction on spinal cords to measure MLR and MLR-associated NTRs. Spinal cord homogenates from hSOD1$^{G93A}$/SynCav1$^+$ mice contained higher Cav-1 protein expression [1-way ANOVA, $F_{(2, 9)}$ = 116.5; $P < 0.0001$; with Tukey's *post hoc*, $n$ = 4/group] with no difference in total TrkB [$F_{(2, 9)}$ = 1.06; $P$ = 0.4] (**Fig. 5***A, B*). hSOD1$^{G93A}$ mice expressed less MLR-localized TrkB [1-way ANOVA, $F_{(2, 9)}$ = 9.5; $P$ = 0.006; with Tukey's *post hoc*] compared with Tg-neg ($P$ = 0.009) and hSOD1$^{G93A}$/SynCav1$^+$ ($P$ = 0.02) (Fig. 5*C, D*). Furthermore, hSOD1$^{G93A}$/SynCav1$^+$ exhibited increased expression of the MLR marker, CT-B [1-way ANOVA, $F_{(2, 9)}$ = 11.8; $P$ = 0.003; with Tukey's *post hoc*] in MLR fractions compared with hSOD1$^{G93A}$ ($P$ = 0.008) and Tg-neg mice ($P$ = 0.005).

## hSOD1$^{G93A}$/SynCav1$^+$ mice exhibited preserved mitochondrial morphology

Mitochondrial alterations and dysfunction have been implicated in ALS (22, 23). Previous work from our group has suggested a novel protective role of Cav-1 in mitochondrial

function (29, 30). Because hSOD1$^{G93A}$/SynCav1$^+$ mice exhibit preserved motor function, α-motor neuron survival, and longer survival, we performed mitochondrial morphometric analysis using EM. Lumbar L4 ventral horn motor neurons from symptomatic 12-wk-old hSOD1$^{G93A}$ mice revealed damaged mitochondria with disorganized cristae, matrix swelling and vacuoles, and abnormal distension between inner and outer mitochondrial membranes (**Fig. 6***A*). Quantitation revealed that hSOD1$^{G93A}$ mice exhibited increased cristae area density fraction [1-way ANOVA, $F_{(3, 147)}$ = 48.3; $P < 0.0001$; with Tukey's *post hoc*, $n$ = 3 mice/group], increased mitochondrial area [$F_{(3, 569)}$ = 175.9; $F_{(2, 454)}$ = 152.5; $P < 0.0001$; $P < 0.0001$], and increased parameter [$F_{(3, 582)}$ = 205.6; $P < 0.0001$] (Fig. 6*B*) in L4 ventral horn motor neurons. In contrast, hSOD1$^{G93A}$/SynCav1$^+$ mice exhibited mitochondrial morphology similar to that seen in Tg-neg controls (no significant difference between hSOD1$^{G93A}$/SynCav1$^+$ and Tg-neg). Further analyses revealed that SynCav1$^+$ mice exhibited cristae area density fraction similar to that of Tg-neg, and hSOD1$^{G93A}$/SynCav1$^+$ and significantly less *vs.* hSOD1$^{G93A}$ ($P < 0.0001$). Tukey's multiple comparison test revealed SynCav1$^+$ mice exhibited significantly smaller mitochondrial area *vs.* hSOD1$^{G93A}$ ($P < 0.0001$) and hSOD1$^{G93A}$/SynCav1$^+$ ($P < 0.0001$) and smaller
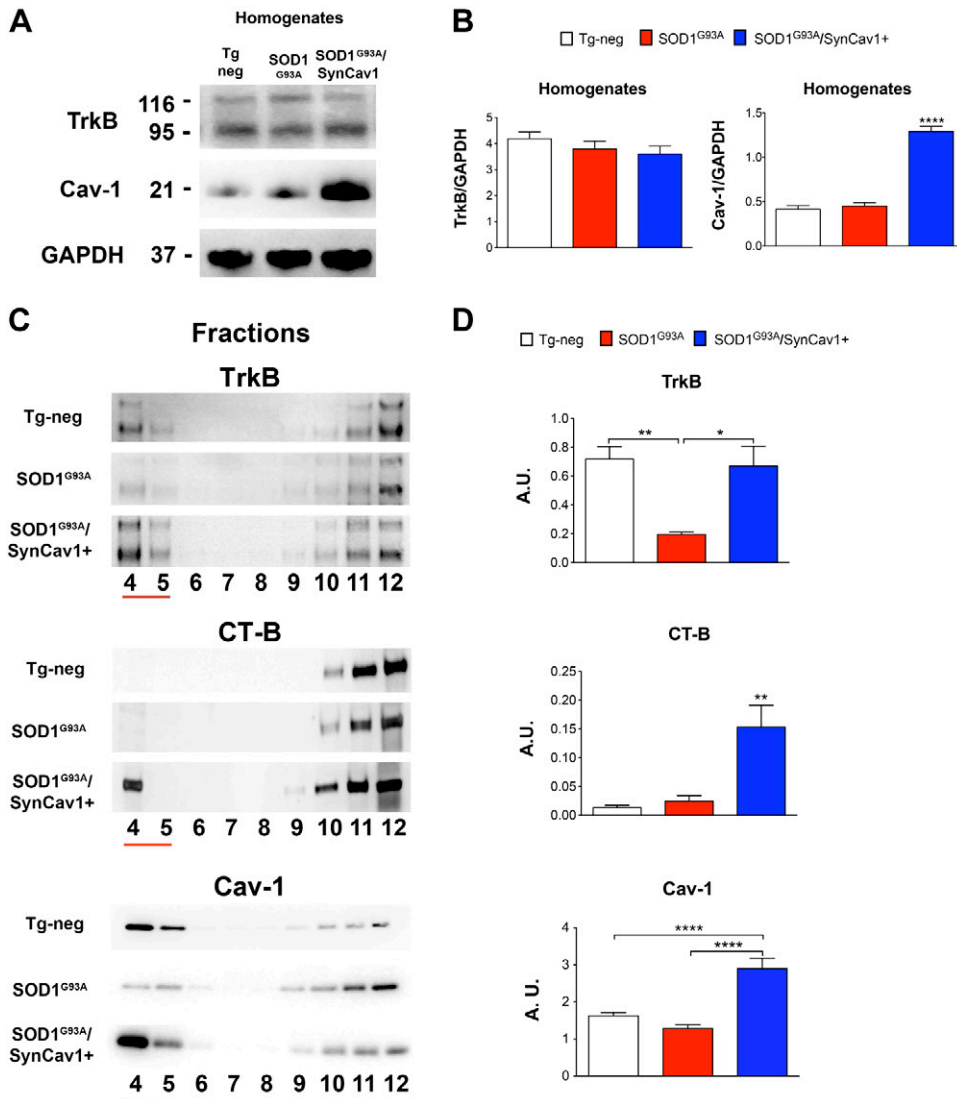
**Figure 5.** SOD1<sup>G93A</sup>/SynCav1<sup>+</sup> mice have increased MLR and MLR-localized TrkB in spinal cord tissue. *A*) Immunoblot of TrkB, Cav-1, and glyceraldehyde-3-phosphate dehydrogenase (GAPDH) in spinal cord homogenates from Tg-neg, SOD1$^{G93A}$, and SOD1$^{G93A}$/SynCav1$^+$ at 12 wk. *B*) quantitation of data in *A*. *C*) Spinal cord tissue subjected to sucrose density fractionation followed by immunoblot of TrkB, CT-B, and Cav-1. *D*) quantitation of data in *C*. All fractions (4–12) were generated from equal protein loading of 0.5 mg/ml. Red line indicates buoyant fractions 4 and 5. Data represent arbitrary units (A.U.) means ± SEM. ($n$ = 4/group). One-way ANOVA with Tukey's multiple comparisons *post hoc* test with significance set at $P < 0.05$. *$P < 0.05$, **$P < 0.01$, ****$P < 0.0001$.

parameter *vs.* hSOD1$^{G93A}$ ($P < 0.0001$), hSOD1$^{G93A}$/SynCav1$^+$ ($P < 0.0001$), and Tg-neg ($P < 0.0001$).

## DISCUSSION

Although previous work from our group demonstrated that neuron-targeted overexpression of Cav-1 *in vivo* augments structural and functional neuroplasticity and improves neurobehavioral outcomes, the functional significance of *SynCav1* in the setting of neurodegeneration had not been investigated. The present study is the first to demonstrate that overexpression of the MLR protein Cav-1, specifically in neurons, extends survival and preserves neuromuscular function in hSOD1$^{G93A}$ mice. Moreover, *SynCav1*-mediated preservation of TrkB expression and localization to MLR microdomains in hSOD1$^{G93A}$ spinal cord tissue, a subcellular event necessary for functional TrkB signaling, nerve growth cone motility, and synaptic modulation (9, 31, 32), may partly identify the molecular mechanism by which *SynCav1* delays ALS progression.

Most ALS-directed therapies are focused on deletion (6, 33) or re-expression of genes (21) that are linked to the

disease of known genetic etiology. Although these approaches show much promise in the setting of FALS, attempts to combat the lesser-known etiology of SALS remain evasive. FALS and SALS exhibit commonality (*i.e.*, degenerating α-motor neurons, decreased neuronal function, and early mortality). Therefore, until the pathologic mechanisms contributing to SALS are fully known, strategies that focus directly on neuroprotection and neuroregeneration (34) may prove effective in delaying disease progression and prolonging survival. Because *SynCav1* enhances MLR localization of neuroprotective NTRs in the brain (13) and spinal cord, this novel gene therapy approach may work synergistically with exogenously administered or already existing endogenous neurotrophins. *SynCav1* gene therapy and these previously mentioned combinatorial approaches show great promise in combating this devastating neurodegenerative motor disease.

Previous work from our group demonstrated, at minimum, 12 mo of gene expression using a 1-time intraparenchymal dose of adeno-associated virus serotype 9 (AAV9)–SynCav1 (19). Intrathecal delivery, direct spinal cord, and brain injections have all demonstrated safety.
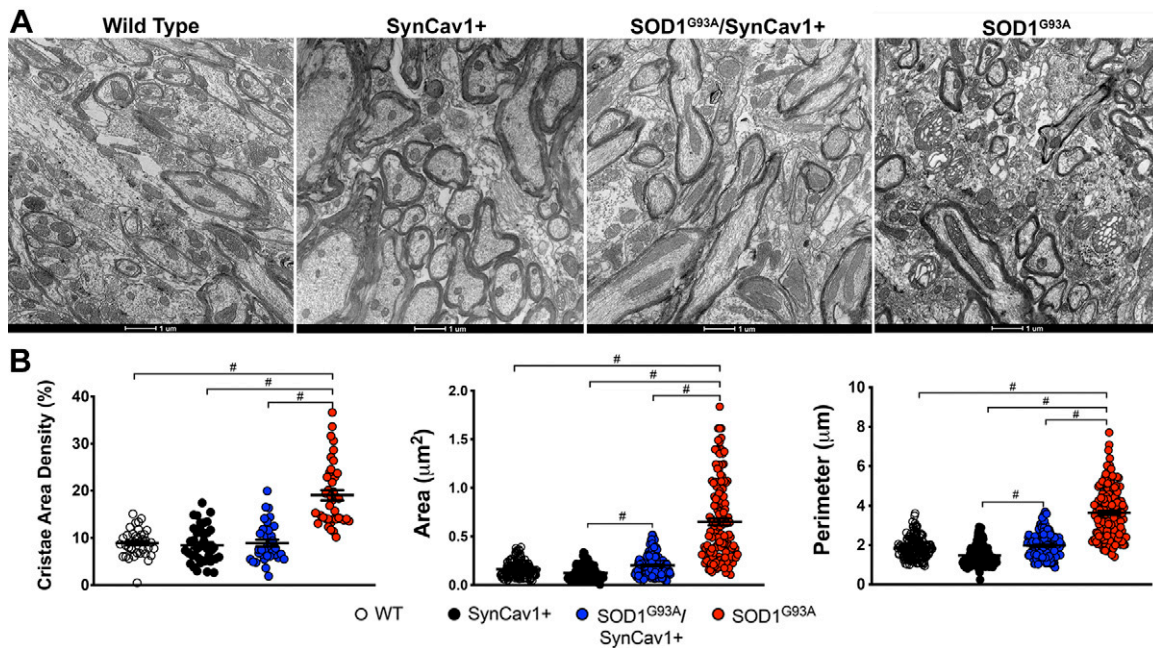
**Figure 6.** SOD1$^{G93A}$/SynCav1$^{+}$ mice exhibit preserved mitochondrial morphology L4 ventral horn motor neurons. *A)* Electron micrographs of motor neuron mitochondria cross sections of spinal cords from lumbar L4 ventral horn of wild-type (Tg-neg; first panel), hSOD1$^{G93A}$ (second panel), SynCav1$^{+}$ (third panel), and hSOD1$^{G93A}$/SynCav1$^{+}$ (fourth panel) mice. Scale bars, 1 μm. *B)* Quantitation of average cristae area density, mitochondrial perimeter, and area. Data represent means ± SEM. (*n* = 3/group). One-way ANOVA with Tukey's multiple comparisons *post hoc* test with significance set at $P < 0.05$. $^{\#}P < 0.05$.

Presently, there are several viral-mediated gene-therapy clinical trials for neurodegenerative diseases (3), and recent intracisternal AAV delivery in nonhuman primates demonstrated wide transgene expression (35). In December 2017, the Food and Drug Administration approved the first-ever AAV-mediated gene therapy for retinal dystrophy, demonstrating a monumental shift in CNS therapies. Synapsin promoter can be used with AAV to drive strong neuron-specific transgene expression in ChAT-positive motor neurons (36), lending justification for future studies to test the potential therapeutic application of *AAV9-SynCav1* in ALS and other neurodegenerative models.

Restoring neuronal connectivity (*i.e.*, neurite extension, growth cone advancement, and synapse formation) is dependent on axonal transport of neurotrophin/NTR complexes from nerve terminals back to the cell body (retrograde) and *vice versa* (anterograde) (37, 38). Under normal cellular conditions, retrograde transport occurs when neurotrophins bind to plasmalemmal NTRs (TrkA, TrkB) followed by endocytosis and attachment to microtubules to facilitate intracellular transport down the axon. Evidence shows that impaired retrograde axonal transport occurs in many neurodegenerative conditions, such as Alzheimer disease, Parkinson disease, ALS, and anesthetic neurotoxicity (39–43). Neurotrophin/Trk signaling, growth cone motility, and synaptic modulation is dependent on MLRs (9, 31, 32). Findings from the present study demonstrating *SynCav1*-increased MLRs and MLR-localized TrkB in hSOD1$^{G93A}$ spinal cords suggest that *SynCav1* may be protecting motor neurons and neuromuscular function, in part, by restoring axonal transport of neurotrophin-NTR signaling endosomes, a subcellular mechanism and hypothesis needing further investigation.

In addition to housing synaptic signaling complexes, MLRs are also enriched in monosialotetrahexosylganglioside (GM1) gangliosides (12). The present study demonstrated an increase in CT-B binding to MLR fractions in hSOD1$^{G93A}$/SynCav1$^{+}$ spinal cords, indicating more GM1 gangliosides. Interestingly, previous clinical trials demonstrated that treating patients with acute spinal cord injury with a GM1 ganglioside drug (termed Sygen) improved neurologic function 1 yr postinjury (44, 45). Although the authors hypothesized that GM1 treatment enhanced white matter, rather than gray matter, the exact mechanism of neuronal recovery was never demonstrated, and debate exists as to whether GM1 is a suitable treatment for spinal cord injury or degeneration (46). Increased MLRs and MLR-associated GM1 gangliosides are neuroprotective and may serve to enhance neuronal survival and axonal function, thus extending the time needed for repair or remyelination after injury or during neurodegenerative conditions. Previous work from our group showed that *SynCav1* increases CT-B and dendritic growth in neurons *in vitro* (15), increases MLR-associated CT-B and dendritic arborization in the hippocampus *in vivo* (13), and increases myelin fiber content in cornu ammonis Schaffer collateral axons (24); however, whether *SynCav1* enhances communication between axons and adjacent oligodendrocytes to preserve axonal function remains unknown.

There are concerns regarding failed clinical trials involving neurotrophin therapy for ALS (47). Several potential reasons such as short half-life *in vivo*, inability to reach target tissue, or broad off-target effects (*e.g.*, unintended p75NTR activation leading to axonal pruning and cell death) could explain for these failed trials (48). A limitation to the present study is that we did not directly measure TrkB

activity nor test the efficacy of TrkB agonists in terms of improved neuromuscular function and extended life span. However, others have shown that neurotrophin analogs, such as 7,8 dihydroxyflavone, can promote axonal growth and improve motor function in models of ALS (49), spinal cord injury (50), and Parkinson disease (51). Because functional TrkB signaling (as well as other NTRs) is dependent on localization to MLRs, the preservation of MLRs and, specifically, TrkB-localization to MLRs in the spinal cord of hSOD1G93A/SynCav1$^+$ mice suggest that *SynCav1* gene delivery may work synergistically to improve the efficacy and potency of TrkB and other NTR agonists for treating individuals afflicted by FALS, SALS, or other forms of neurodegeneration of unknown origin.

There are several limitations to the current study, such as the sole use of 1 sex (*i.e.*, male mice), only 1 ALS transgenic model was tested (hSOD1$^{G93A}$), and the use of a SynCav1 transgenic mouse only provides a preventative proof of concept rather than a disease-modifying intervention after disease onset. However, researchers are obligated to first demonstrate proof-of-concept results with the use of potential disease-modifying interventions prior to testing different dosing regimens and/or routes of delivery (*e.g.*, intraventricular, subpial, intraparenchymal) to properly test biologics in other forms of ALS or other indications (*e.g.*, motor neuron disease, Alzheimer disease, and Parkinson disease). We have therefore initiated future studies to test whether exogenous delivery of *AAV9-SynCav1* to both male and female hSOD1$^{G93A}$ mice can demonstrate similar neuroprotective results (*i.e.*, restoration of neuromuscular function, preservation of body weight, and extended longevity) and eagerly await these results. **FJ**

## AUTHOR CONTRIBUTIONS

A. Sawada, S. Wang, and M. Jian performed research and analyzed data; J. Leem performed genotyping and animal colony maintenance for experiments; J. Wackerbarth and J. Egawa performed MEP and EMG experiments; J. Schilling analyzed data; O. Platoshyn analyzed MEP and EMG data; A. Zemljic-Harpf assisted with EM; D. M. Roth, H. H. Patel, and P. M. Patel assisted with writing the manuscript; M. Marsala assisted with experimental design; and B. P. Head designed the research, performed EM imaging and analysis, and wrote the manuscript.

## REFERENCES

1. Kiernan, M. C., Vucic, S., Cheah, B. C., Turner, M. R., Eisen, A., Hardiman, O., Burrell, J. R., and Zoing, M. C. (2011) Amyotrophic lateral sclerosis. *Lancet* **377**, 942–955
2. Keifer, O. P., Jr., O'Connor, D. M., and Boulis, N. M. (2014) Gene and protein therapies utilizing VEGF for ALS. *Pharmacol. Ther.* **141**, 261–271
3. O'Connor, D. M., and Boulis, N. M. (2015) Gene therapy for neurodegenerative diseases. *Trends Mol. Med.* **21**, 504–512; erratum: **22**, 266
4. Brown, R. H., and Al-Chalabi, A. (2017) Amyotrophic lateral sclerosis. *N. Engl. J. Med.* **377**, 162–172
5. Hardiman, O., and van den Berg, L. H. (2017) Edaravone: a new treatment for ALS on the horizon? *Lancet Neurol.* **16**, 490–491
6. Ajroud-Driss, S., and Siddique, T. (2015) Sporadic and hereditary amyotrophic lateral sclerosis (ALS). *Biochim. Biophys. Acta* **1852**, 679–684
7. Tovar-Y-Romo, L. B., Ramírez-Jarquín, U. N., Lazo-Gómez, R., and Tapia, R. (2014) Trophic factors as modulators of motor neuron physiology and survival: implications for ALS therapy. *Front. Cell. Neurosci.* **8**, 61
8. Silva-Hucha, S., Hernández, R. G., Benítez-Temiño, B., Pastor, A. M., de la Cruz, R. R., and Morcuende, S. (2017) Extraocular motoneurons of the adult rat show higher levels of vascular endothelial growth factor and its receptor Flk-1 than other cranial motoneurons. *PLoS One* **12**, e0178616
9. Suzuki, S., Numakawa, T., Shimazu, K., Koshimizu, H., Hara, T., Hatanaka, H., Mei, L., Lu, B., and Kojima, M. (2004) BDNF-induced recruitment of TrkB receptor into neuronal lipid rafts: roles in synaptic modulation. *J. Cell Biol.* **167**, 1205–1215
10. Guirland, C., and Zheng, J. Q. (2007) Membrane lipid rafts and their role in axon guidance. *Adv. Exp. Med. Biol.* **621**, 144–155
11. Romanelli, R. J., Mahajan, K. R., Fulmer, C. G., and Wood, T. L. (2009) Insulin-like growth factor-I-stimulated Akt phosphorylation and oligodendrocyte progenitor cell survival require cholesterol-enriched membranes. *J. Neurosci. Res.* **87**, 3369–3377
12. Head, B. P., Patel, H. H., and Insel, P. A. (2014) Interaction of membrane/lipid rafts with the cytoskeleton: impact on signaling and function: membrane/lipid rafts, mediators of cytoskeletal arrangement and cell signaling. *Biochim. Biophys. Acta.* **1838**, 532–545
13. Mandyam, C. D., Schilling, J. M., Cui, W., Egawa, J., Niesman, I. R., Kellerhals, S. E., Staples, M. C., Busija, A. R., Risbrough, V. B., Posadas, E., Grogman, G. C., Chang, J. W., Roth, D. M., Patel, P. M., Patel, H. H., and Head, B. P. (2017) Neuron-targeted caveolin-1 improves molecular signaling, plasticity, and behavior dependent on the Hippocampus in adult and aged mice. *Biol. Psychiatry* **81**, 101–110
14. Head, B. P., Patel, H. H., Tsutsumi, Y. M., Hu, Y., Mejia, T., Mora, R. C., Insel, P. A., Roth, D. M., Drummond, J. C., and Patel, P. M. (2008) Caveolin-1 expression is essential for N-methyl-D-aspartate receptor-mediated Src and extracellular signal-regulated kinase 1/2 activation and protection of primary neurons from ischemic cell death. *FASEB J.* **22**, 828–840
15. Head, B. P., Hu, Y., Finley, J. C., Saldana, M. D., Bonds, J. A., Miyanohara, A., Niesman, I. R., Ali, S. S., Murray, F., Insel, P. A., Roth, D. M., Patel, H. H., and Patel, P. M. (2011) Neuron-targeted caveolin-1 protein enhances signaling and promotes arborization of primary neurons. *J. Biol. Chem.* **286**, 33310–33321
16. Howland, D. S., Liu, J., She, Y., Goad, B., Maragakis, N. J., Kim, B., Erickson, J., Kulik, J., DeVito, L., Psaltis, G., DeGennaro, L. J., Cleveland, D. W., and Rothstein, J. D. (2002) Focal loss of the glutamate transporter EAAT2 in a transgenic rat model of SOD1 mutant-mediated amyotrophic lateral sclerosis (ALS). *Proc. Natl. Acad. Sci. USA* **99**, 1604–1609
17. Zhong, Z., Ilieva, H., Hallagan, L., Bell, R., Singh, I., Paquette, N., Thiyagarajan, M., Deane, R., Fernandez, J. A., Lane, S., Zlokovic, A. B., Liu, T., Griffin, J. H., Chow, N., Castellino, F. J., Stojanovic, K., Cleveland, D. W., and Zlokovic, B. V. (2009) Activated protein C therapy slows ALS-like disease in mice by transcriptionally inhibiting SOD1 in motor neurons and microglia cells. *J. Clin. Invest.* **119**, 3437–3449

18. Ludolph, A. C., Bendotti, C., Blaugrund, E., Chio, A., Greensmith, L., Loeffler, J. P., Mead, R., Niessen, H. G., Petri, S., Pradat, P. F., Robberecht, W., Ruegg, M., Schwalenstöcker, B., Stiller, D., van den Berg, L., Vieira, F., and von Horsten, S. (2010) Guidelines for preclinical animal research in ALS/MND: a consensus meeting. *Amyotroph. Lateral Scler.* **11**, 38–45

19. Egawa, J., Schilling, J. M., Cui, W., Posadas, E., Sawada, A., Alas, B., Zemljic-Harpf, A. E., Fannon-Pavlich, M. J., Mandyam, C. D., Roth, D. M., Patel, H. H., Patel, P. M., and Head, B. P. (2017) Neuron-specific caveolin-1 overexpression improves motor function and preserves memory in mice subjected to brain trauma. *FASEB J.* **31**, 3403–3411

20. Glover, C. P., Bienemann, A. S., Heywood, D. J., Cosgrave, A. S., and Uney, J. B. (2002) Adenoviral-mediated, high-level, cell-specific transgene expression: a SYN1-WPRE cassette mediates increased transgene expression with no loss of neuron specificity. *Mol. Ther.* **5**, 509–516

21. Song, S., Miranda, C. J., Braun, L., Meyer, K., Frakes, A. E., Ferraiuolo, L., Likhite, S., Bevan, A. K., Foust, K. D., McConnell, M. J., Walker, C. M., and Kaspar, B. K. (2016) Major histocompatibility complex class I molecules protect motor neurons from astrocyte-induced toxicity in amyotrophic lateral sclerosis. *Nat. Med.* **22**, 397–403

22. Parone, P. A., Da Cruz, S., Han, J. S., McAlonis-Downes, M., Vetto, A. P., Lee, S. K., Tseng, E., and Cleveland, D. W. (2013) Enhancing mitochondrial calcium buffering capacity reduces aggregation of misfolded SOD1 and motor neuron cell death without extending survival in mouse models of inherited amyotrophic lateral sclerosis. *J. Neurosci.* **33**, 4657–4671

23. Pasqua, T., Mahata, S., Bandyopadhyay, G. K., Biswas, A., Perkins, G. A., Sinha-Hikim, A. P., Goldstein, D. S., Eiden, L. E., and Mahata, S. K. (2016) Impact of Chromogranin A deficiency on catecholamine storage, catecholamine granule morphology and chromaffin cell energy metabolism in vivo. *Cell Tissue Res.* **363**, 693–712; erratum: 823

24. Egawa, J., Zemljic-Harpf, A., Mandyam, C. D., Niesman, I. R., Lysenko, L. V., Kleschevnikov, A. M., Roth, D. M., Patel, H. H., Patel, P. M., and Head, B. P. (2018) Neuron-targeted caveolin-1 promotes ultrastructural and functional hippocampal synaptic plasticity. *Cereb. Cortex* **28**, 3255–3266

25. Buk, D. M., Waibel, M., Braig, C., Martens, A. S., Heinrich, P. C., and Graeve, L. (2004) Polarity and lipid raft association of the components of the ciliary neurotrophic factor receptor complex in Madin-Darby canine kidney cells. *J. Cell Sci.* **117**, 2063–2075

26. Nathanson, N. M. (2012) Regulation of neurokine receptor signaling and trafficking. *Neurochem. Int.* **61**, 874–878

27. Zonta, B., and Minichiello, L. (2013) Synaptic membrane rafts: traffic lights for local neurotrophin signaling? *Front. Synaptic Neurosci.* **5**, 9

28. Laurenzana, A., Fibbi, G., Chillà, A., Margheri, G., Del Rosso, T., Rovida, E., Del Rosso, M., and Margheri, F. (2015) Lipid rafts: integrated platforms for vascular organization offering therapeutic opportunities. *Cell. Mol. Life Sci.* **72**, 1537–1557

29. Fridolfsson, H. N., Kawaraguchi, Y., Ali, S. S., Panneerselvam, M., Niesman, I. R., Finley, J. C., Kellerhals, S. E., Migita, M. Y., Okada, H., Moreno, A. L., Jennings, M., Kidd, M. W., Bonds, J. A., Balijepalli, R. C., Ross, R. S., Patel, P. M., Miyanohara, A., Chen, Q., Lesnefsky, E. J., Head, B. P., Roth, D. M., Insel, P. A., and Patel, H. H. (2012) Mitochondria-localized caveolin in adaptation to cellular stress and injury. *FASEB J.* **26**, 4637–4649

30. Wang, J., Schilling, J. M., Niesman, I. R., Headrick, J. P., Finley, J. C., Kwan, E., Patel, P. M., Head, B. P., Roth, D. M., Yue, Y., and Patel, H. H. (2014) Cardioprotective trafficking of caveolin to mitochondria is Gi-protein dependent. *Anesthesiology* **121**, 538–548

31. Guirland, C., Suzuki, S., Kojima, M., Lu, B., and Zheng, J. Q. (2004) Lipid rafts mediate chemotropic guidance of nerve growth cones. *Neuron* **42**, 51–62

32. Suzuki, S., Kiyosue, K., Hazama, S., Ogura, A., Kashihara, M., Hara, T., Koshimizu, H., and Kojima, M. (2007) Brain-derived neurotrophic factor regulates cholesterol metabolism for synapse development. *J. Neurosci.* **27**, 6417–6427

33. Boillée, S., and Cleveland, D. W. (2008) Revisiting oxidative damage in ALS: microglia, Nox, and mutant SOD1. *J. Clin. Invest.* **118**, 474–478

34. Hefferan, M. P., Galik, J., Kakinohana, O., Sekerkova, G., Santucci, C., Marsala, S., Navarro, R., Hruska-Plochan, M., Johe, K., Feldman, E., Cleveland, D. W., and Marsala, M. (2012) Human neural stem cell replacement therapy for amyotrophic lateral sclerosis by spinal transplantation. *PLoS One* **7**, e42614

35. Rosenberg, J. B., Kaplitt, M. G., De, B. P., Chen, A., Flagiello, T., Salami, C., Pey, E., Zhao, L., Ricart Arbona, R. J., Monette, S., Dyke, J. P., Ballon, D. J., Kaminsky, S. M., Sondhi, D., Petsko, G. A., Paul, S. M., and Crystal, R. G. (2018) AAVrh.10-mediated APOE2 central nervous system gene therapy for APOE4-associated Alzheimer's disease. *Hum. Gene Ther. Clin. Dev.* **29**, 24–47

36. McLean, J. R., Smith, G. A., Rocha, E. M., Hayes, M. A., Beagan, J. A., Hallett, P. J., and Isacson, O. (2014) Widespread neuron-specific transgene expression in brain and spinal cord following synapsin promoter-driven AAV9 neonatal intracerebroventricular injection. *Neurosci. Lett.* **576**, 73–78

37. Bartlett, S. E., Reynolds, A. J., and Hendry, I. A. (1998) Retrograde axonal transport of neurotrophins: differences between neuronal populations and implications for motor neuron disease. *Immunol. Cell Biol.* **76**, 419–423

38. Yamashita, N., and Kuruvilla, R. (2016) Neurotrophin signaling endosomes: biogenesis, regulation, and functions. *Curr. Opin. Neurobiol.* **39**, 139–145

39. Stokin, G. B., Lillo, C., Falzone, T. L., Brusch, R. G., Rockenstein, E., Mount, S. L., Raman, R., Davies, P., Masliah, E., Williams, D. S., and Goldstein, L. S. (2005) Axonopathy and transport deficits early in the pathogenesis of Alzheimer's disease. *Science* **307**, 1282–1288

40. Stokin, G. B., and Goldstein, L. S. (2006) Axonal transport and Alzheimer's disease. *Annu. Rev. Biochem.* **75**, 607–627

41. Chevalier-Larsen, E., and Holzbaur, E. L. (2006) Axonal transport and neurodegenerative disease. *Biochim. Biophys. Acta* **1762**, 1094–1108

42. Millecamps, S., and Julien, J. P. (2013) Axonal transport deficits and neurodegenerative diseases. *Nat. Rev. Neurosci.* **14**, 161–176

43. Pearn, M. L., Schilling, J. M., Jian, M., Egawa, J., Wu, C., Mandyam, C. D., Fannon-Pavlich, M. J., Nguyen, U., Bertoglio, J., Kodama, M., Mahata, S. K., DerMardirossian, C., Lemkuil, B. P., Han, R., Mobley, W. C., Patel, H. H., Patel, P. M., and Head, B. P. (2018) Inhibition of RhoA reduces propofol-mediated growth cone collapse, axonal transport impairment, loss of synaptic connectivity, and behavioural deficits. *Br. J. Anaesth.* **120**, 745–760

44. Geisler, F. H., Dorsey, F. C., and Coleman, W. P. (1993) Past and current clinical studies with GM-1 ganglioside in acute spinal cord injury. *Ann. Emerg. Med.* **22**, 1041–1047

45. Geisler, F. H. (1993) GM-1 ganglioside and motor recovery following human spinal cord injury. *J. Emerg. Med.* **11** (Suppl 1), 49–55

46. Haller, J., Bice, M., and Lawrence, B. (2016) Mediating the secondary effects of spinal cord injury through optimization of key physiologic parameters. *J. Am. Acad. Orthop. Surg.* **24**, 160–171

47. Saragovi, H. U., Hamel, E., and Di Polo, A. (2009) A neurotrophic rationale for the therapy of neurodegenerative disorders. *Curr. Alzheimer Res.* **6**, 419–423

48. Brahimi, F., Maira, M., Barcelona, P. F., Galan, A., Aboulkassim, T., Teske, K., Rogers, M. L., Bertram, L., Wang, J., Yousefi, M., Rush, R., Fabian, M., Cashman, N., and Saragovi, H. U. (2016) The paradoxical signals of two TrkC receptor isoforms supports a rationale for novel therapeutic strategies in ALS. *PLoS One* **11**, e0162307

49. Korkmaz, O. T., Aytan, N., Carreras, I., Choi, J. K., Kowall, N. W., Jenkins, B. G., and Dedeoglu, A. (2014) 7,8-Dihydroxyflavone improves motor performance and enhances lower motor neuronal survival in a mouse model of amyotrophic lateral sclerosis. *Neurosci. Lett.* **566**, 286–291

50. English, A. W., Liu, K., Nicolini, J. M., Mulligan, A. M., and Ye, K. (2013) Small-molecule trkB agonists promote axon regeneration in cut peripheral nerves. *Proc. Natl. Acad. Sci. USA* **110**, 16217–16222

51. Jang, S. W., Liu, X., Yepes, M., Shepherd, K. R., Miller, G. W., Liu, Y., Wilson, W. D., Xiao, G., Blanchi, B., Sun, Y. E., and Ye, K. (2010) A selective TrkB agonist with potent neurotrophic activities by 7,8-dihydroxyflavone. *Proc. Natl. Acad. Sci. USA* **107**, 2687–2692